

Effects of functional group mass variance on vibrational properties and thermal transport in graphene

L. Lindsay¹ and Y. Kuang^{2*}

¹Materials Science and Technology Division, Oak Ridge National Laboratory, Oak Ridge, Tennessee 37831, USA

²School of Mechanics and Construction Engineering, Jinan University, Guangzhou, China

*co-first author (equal contributions to work)

This manuscript has been authored by UT-Battelle, LLC under Contract No. DE-AC05-00OR22725 with the U.S. Department of Energy. The United States Government retains and the publisher, by accepting the article for publication, acknowledges that the United States Government retains a non-exclusive, paid-up, irrevocable, world-wide license to publish or reproduce the published form of this manuscript, or allow others to do so, for United States Government purposes. The Department of Energy will provide public access to these results of federally sponsored research in accordance with the DOE Public Access Plan(<http://energy.gov/downloads/doe-public-access-plan>).

Effects of functional group mass variance on vibrational properties and thermal transport in graphene

L. Lindsay¹ and Y. Kuang^{2*}

¹Materials Science and Technology Division, Oak Ridge National Laboratory, Oak Ridge, Tennessee 37831, USA

² School of Mechanics and Construction Engineering, Jinan University, Guangzhou, China

Abstract

Intrinsic thermal resistivity critically depends on features of phonon dispersions dictated by harmonic interatomic forces and masses. Here we present the effects of functional group mass variance on vibrational properties and thermal conductivity (κ) of functionalized graphene from first principles calculations. We use graphane, a buckled graphene backbone with covalently bonded Hydrogen atoms on both sides, as the base material and vary the mass of the Hydrogen atoms to simulate the effect of mass variance from other functional groups. We find non-monotonic behavior of κ with increasing mass of the functional group and an unusual cross-over from acoustic-dominated to optic-dominated thermal transport behavior. We connect this cross-over to changes in the phonon dispersion with varying mass which suppress acoustic phonon velocities, but also give unusually high velocity optic modes. Further, we show that out-of-plane acoustic vibrations contribute significantly more to thermal transport than in-plane acoustic modes despite breaking of a reflection symmetry based scattering selection rule responsible for their large contributions in graphene. This work demonstrates the potential for manipulation and engineering of thermal transport properties in two dimensional materials toward targeted applications.

*co-first author (equal contributions to work)

I. INTRODUCTION

Two-dimensional (2D) materials continue to intrigue scientific and engineering communities with the variety of interesting fundamental properties and possible applications (varying electronic behaviors [1-5], observations of quantum effects [6], transistors [4], etc.) that can be obtained in a now wide range of systems, e.g., graphene [1-3], silicene [7], borophene [8], phosphorenes [5], transition metal dichalcogenides [4, 9], just to name a few. Significant research interest has been devoted to functionalizing 2D systems, graphene in particular [10-12], to engineer these properties (e.g., electronic band gap [13], chemical reactivity [14]) for targeted applications in a variety of electronics and chemical delivery systems. Here we examine the effects of varying mass on vibrational and thermal transport properties of functionalized graphene systems.

Suspended graphene has been reported to have extremely high values for thermal conductivity κ ranging from 2000-5300 W/m-K [15-19]. However, interaction of single-layer graphene with a supporting substrate [20] and with polymer residue [21] can provide significant thermal resistance. The high κ of graphene and this reduction of κ with substrate interaction can be partly understood in terms of large contributions to κ from out-of-plane flexural acoustic (ZA) phonons. In purely flat graphene a scattering selection rule based on reflection symmetry gives significantly reduced scattering of such phonons, which thus contribute significantly to thermal transport [22]. The influence of a supporting substrate [20], other layers [23, 24] and curvature [25] all break this selection rule to some degree, giving more scattering of ZA phonons and lower κ . Chemical functionalization also breaks reflection symmetry of graphene, even in fully-functionalized crystalline systems, with the presence of covalently bonded atomic groups on the surfaces and buckling of the Carbon backbone (no longer strictly sp^2 hybridized). Recent first

principles calculations gave ~ 2 times reduction of κ for graphane compared to graphene, and found a further κ reduction when comparing to a heavier mass fluorinated graphene system [26]. It was argued that changes in the phonon dispersion play the dominant role in the κ reduction going from graphane to fluorographene.

Motivated by that work, here we present first principles κ calculations of graphane with varying mass of the Hydrogen atoms to simulate the effects of other functional group masses on graphene κ . In Section II we briefly outline details of the theory and numerical methods employed here. Section III gives the results of our calculations and discussion of these, while Section IV summarizes this work.

II. THEORETICAL METHODS

The structure of fully-covered functionalized graphene systems is shown in the inset to Fig. 1. We note that these systems are crystalline, no phonon-defect scattering included. These systems have the same hexagonal structure as graphene; however, the functional groups that alternately bond to the top and bottom buckle the Carbon backbone. The electronic structure of graphane ($C^{-1}H$) was determined within density functional theory [28, 29] using the Quantum Espresso package [30, 31] within the local density approximation (LDA) with Perdew-Zunger exchange correlation [32] and Von Barth-Car pseudopotentials [33] for core electrons. A $13 \times 13 \times 1$ k -mesh, >30 Å vacuum space and 120 Rydberg plane wave energy cutoff were used to determine lattice constant = 2.501 Å, buckling height = 0.448 Å and C-H distance = 1.114 Å by energy minimization. These are slightly smaller than those found in Ref. 34 which employed the generalized gradient approximation. LDA calculations typically bind atoms more strongly than GGA [35]. Dispersion interactions are not included as all atoms are covalently bonded and only single-layer systems are considered.

Harmonic and third-order anharmonic interatomic force constants (IFCs) of graphane were determined by numerical differentiation from forces calculated in perturbed supercells of 324 atoms using Γ -point-only, 100 Rydberg plane wave energy cutoff electronic structure calculations with a 28 Å vacuum distance between periodic layers. Finite numerical differences and truncated atomic interactions require that various symmetries be enforced on ‘raw’ IFCs [36-38]. Specifically, small changes are applied to the ‘raw’ harmonic and anharmonic IFCs via a χ^2 minimization procedure [36, 39] to ensure that all point group symmetries and translational invariance conditions are enforced [40, 41]. Further, Born-Huang equilibrium invariance constraints [42] are also imposed on the harmonic IFCs.

For each system these graphane harmonic and anharmonic IFCs were used, thus differences in phonon scattering and κ arise only from changes in the H atom mass that enters the scattering matrix elements and the dynamical matrix:

$$D_{\alpha\beta}^{kk'}(\vec{q}) = \frac{1}{\sqrt{m_\sigma m_{\sigma'}}} \sum_{l'} \Phi_{\alpha\beta}^{0\sigma,l'\sigma'} e^{i\vec{q}\cdot\vec{R}_l} \quad (1)$$

where \vec{q} is the phonon wave vector, \vec{R}_l is the lattice vector locating the l th unit cell, m_σ is the mass of the σ th atom, α and β are Cartesian components and $\Phi_{\alpha\beta}^{0\sigma,l'\sigma'}$ are harmonic IFCs. We note that the masses of the Carbon atoms still play an important role in governing the dispersion and scattering, particularly for the acoustic modes of the lighter systems. For the graphane systems considered here the unit cell comprises two Carbon atoms in the buckled backbone and two attached Hydrogen atoms for which their mass is varied for each system. This gives two in-plane acoustic branches with linear dispersion, transverse (TA) and longitudinal (LA), and nine optic branches. There is also a flexural acoustic (ZA) branch with quadratic dispersion characteristically found in 2D systems [38, 43, 44]. Obtaining a perfectly quadratic branch can

be difficult due to numerical inaccuracies of ‘raw’ harmonic IFCs; however, application of Born-Huang equilibrium invariance constraints [42] naturally gives this feature in 2D systems.

Lattice thermal conductivity is expressed as:

$$\kappa = \kappa_{\alpha\alpha} = \sum_{\bar{q}j} C_{\bar{q}j} v_{\bar{q}j\alpha}^2 \tau_{\bar{q}j\alpha} \quad (2)$$

where $C_{\bar{q}j}$ is the volume normalized mode specific heat and $v_{\bar{q}j\alpha}$ is the α th component of the phonon group velocity, both of which are obtained from phonon dispersions based on the harmonic IFCs. Here, j is the branch index. $\tau_{\bar{q}j\alpha}$ is the transport lifetime obtained from Fermi’s golden rule using anharmonic IFCs and by fully solving the linearized Peierls-Boltzmann transport equation [45-47] with a small temperature gradient in the α th direction. Details of the calculations have been described previously [22, 36, 37]. The summations in Eq. 2 and in the scattering rate calculations [22, 46, 47] are converted to integrals and solved numerically using Gaussian quadrature with 3072 points sampled in the first Brillouin zone. The layer thickness required to determine volume is taken as that typically defined for graphene, 3.35 Å. The first principles κ calculations presented here were also independently verified using a density functional tight binding method described previously [48].

III. RESULTS AND DISCUSSION

Figure 1 gives calculated room temperature κ of functionalized graphene versus mass of the functional group. Again, harmonic and anharmonic IFCs were calculated for graphane (C-¹H) and are the same for each system presented here. Previously calculated values of κ for graphane and fluorographene [27] compare favorably with those presented here, 6% and 12% differences, respectively. As found in Ref. 27, graphane has ~2 times smaller κ than that calculated for graphene (~3600 W/m-K [49]) and κ decreases significantly with increasing mass of the

functional atom. Increasing mass has the general effect of reducing the overall frequency scale of phonon dispersions, as can be seen in Fig. 2 comparing those of C-¹H, C-²H and C-³H. This tends to give lower velocities to heat-carrying acoustic phonons and more scatterings of these with lower frequency optic branches, both giving reduced κ . This is demonstrated by the red dashed curve in Fig. 1 which gives acoustic mode contributions to the total κ . A striking feature of Fig. 1, however, is the non-monotonic behavior of κ . With increasing mass beyond ³⁰H κ increases from a minimum ~ 235 W/m-K to peak again at ⁷⁵H with $\kappa=410$ W/m-K before slowly decreasing with further increasing mass. More interesting is the origin of this behavior: cross-over from typical acoustic-dominated transport at small mass to unusual optic-dominated transport at large mass. Very recently κ governed by optic phonons has been reported in the complex phase change material Ge₂Sb₂Te₅ and was attributed to highly dispersive optic branches [50]. *Is the origin of this behavior similar for the simpler 2D systems presented here? How does this behavior evolve with increasing mass of the functional atoms?*

To further elucidate the origin of optic phonon contributions to κ , Fig. 3 gives the accumulated κ with increasing frequency for a subset of systems here. Each curve is scaled by the overall κ of the corresponding system. Figure 3 demonstrates the frequency ranges that provide significant contributions to κ for each phonon spectrum. For instance, for ⁶⁰H $\sim 25\%$ of κ comes from acoustic modes below 5 THz, while $\sim 75\%$ are coming from optic modes between 15 and 25 THz. To correlate the changes in κ and κ accumulation with varying mass, and thus varying phonon frequencies, Fig. 4 gives the dispersion of these systems in the $\Gamma \rightarrow M$ direction for the LA branch and the two most dispersive optic branches in the spectrum; Table I gives the magnitude of the phonon velocities for the LA (Γ) mode and the most dispersive optical branch at the M/2 point along the $\Gamma \rightarrow M$ direction for select systems. The lightest systems considered,

C-¹H, C-²H and C-³H, have very large zone-center LA phonon speeds (Table I), characteristic of light systems with strong covalent bonding. The most dispersive optic modes in these lightest systems have much smaller speeds. For this reason, as is typically the case, the acoustic phonons carry more heat than optic phonons. However, as mass continues to increase a curious cross-over occurs: these optic modes become more dispersive than the acoustic modes, thus have higher velocities. With increasing mass the zone-center LA velocities continuously decrease, while optic phonon velocities continuously increase, as shown in Table I and by Fig.4. Some optic modes are nearly twice as fast as LA modes. For this reason, large contributions to the accumulated κ of Fig. 3 occur in frequency ranges of larger mass materials where these optic branches are most dispersive. We note that the trend given by the LA branches, decreasing velocity with increasing mass, holds for all three acoustic branches.

The optic branches become more dispersive with increasing mass of the functional atoms because zone center frequencies decrease, while zone boundary modes have relatively constant frequency. In striving for deeper understanding of the mechanisms of this behavior it is instructive to map the frequencies of the governing phonon modes to a simple mass/spring harmonic oscillator model. For such a model the frequency is given by $\omega = A\sqrt{k_{eff} / m_{eff}}$ where A is a constant, k_{eff} is an effective spring constant (governed by harmonic IFCs), and m_{eff} is the effective mass of the system. Here we define $m_{eff} = \sum_{\sigma} m_{\sigma} |\hat{e}_{\bar{q}j\sigma}|^2$ as the sum of unit cell masses weighted by the eigenmotion of the phonon mode where $\hat{e}_{\bar{q}j}$ is the eigenvector. In comparing particular phonon mode frequencies with varying system mass, harmonic IFCs and thus k_{eff} are unaltered, and thus do not contribute to frequency differences. Table I gives the calculated m_{eff} for the LA (M) mode and the Γ and M modes of the most dispersive optic branch for select

systems, as well as phonon frequencies at the Γ and M points for this optic branch. With increasing system mass, m_{eff} for the LA (M) increases significantly thus giving smaller zone boundary frequencies and smaller velocities. Similarly for the optic mode at the Γ point, m_{eff} increases substantially with increasing system mass thus giving significantly decreasing frequencies at this point. However, for the M point m_{eff} increases very little and thus frequencies decrease only slightly, giving an increasingly dispersive optic branch with increasing functional mass.

Although the changing velocities of acoustic (a) and optic (o) phonons with increasing functional mass is the driving factor for κ differences in these systems it is instructive to examine phonon scattering processes, which also play a role. Two features of the dispersions are particularly relevant in this regard: an a - o frequency gap and optic phonon bandwidth, both of which govern the interactions of a and o phonons. Considering energy conservation a large a - o gap limits the amount of scattering for two a phonons with one o phonon (aa scattering) [51-53], while small optic bandwidth limits the amount of ao scattering [54, 55]. For C-¹H there is a relatively small a - o gap despite having a large mass ratio of 12. Thus ~80% of the acoustic modes participate in aa processes, despite previous work that demonstrated aa scattering does not exist in compound semiconductors with mass ratios >4 [53]. This condition, however, depends critically on crystal structure and does not apply to various rocksalt compounds [56], nor to the systems here. As functional atom mass increases the a - o gap relative to the acoustic frequency scale remains relatively constant as both a and o modes shift to lower frequencies. More importantly, the optic bandwidth relative to the acoustic frequency scale becomes larger with increasing functional atom mass. For C-¹H only ~50% of the acoustic phonons can participate in ao processes. For C-²H this goes up to ~75% and for C-³H and the other heavier

systems all acoustic phonons can participate in *ooo* scatterings. Thus, changing optic bandwidth plays a role in the sharp decrease in κ going from C-¹H to C-³H, however, is less important in κ differences with further increasing mass.

The ZA phonons have smaller velocities than those of in-plane modes (LA and TA), but still contribute significantly especially for functional group mass smaller than 35 amu, as shown in Fig. 5 which gives a further breakdown of the mode contributions to the total κ . In graphane the Carbon backbone is buckled and the presence of the Hydrogen groups breaks the reflection symmetry present in purely flat graphene. This breaks a phonon-phonon scattering selection rule [22] and allows for more scattering of ZA phonons than in graphene, thus κ contributions from ZA modes drop from ~ 2700 W/m-K in graphene to ~ 1200 W/m-K in graphane, though drop in the percent contribution to κ in Fig. 5 is not as dramatic. Regardless, in graphane and heavier functional mass systems ZA phonons still contribute the largest share of the acoustic mode contributions to κ , similar to that found in other buckled monolayer systems [57]. To better understand this we note that ZA mode velocities only disappear near the Brillouin zone center. For C-¹H the average ZA phonon speed in the transport direction, ~ 3.81 km/s, is comparable to that of the TA and LA branches, 4.06 km/s and 4.22 km/s, respectively. Further, the average lifetime of the ZA phonons in C-¹H, ~ 18.9 ps, is over an order of magnitude smaller than that of graphene due to relaxing of the selection rule, however, it is still significantly higher than that of the TA and LA phonons, 8.5 ps and 7.1 ps, respectively.

We also made calculations of κ including phonon-isotope scattering from naturally abundant Carbon isotope concentrations (see Fig. 5) via quantum mechanical perturbation theory methods described elsewhere [49, 58, 59]. We find that in all systems, even those with κ contributions

dominated by optic phonons, the additional resistance from naturally-occurring isotopes plays only a minor role in determining κ .

IV. SUMMARY AND CONCLUSIONS

We presented calculations of thermal conductivity (κ) for mass functionalized graphene systems based on Peierls-Boltzmann transport equation methods with harmonic and anharmonic forces from density functional theory. With fully-covered Hydrogen functionalized graphene (also known as graphane) as the base system we examined the effects of mass variance of the H atoms on vibrational and lattice thermal transport properties. Calculations give a non-monotonic behavior of κ with increasing mass that is governed by an unusual cross-over from acoustic-dominated to optic-dominated heat transport. With increasing mass of the functional atoms acoustic mode velocities expectedly decrease, however, particular optic phonon modes have increasing velocity, and thus give larger contributions to κ . Further we show that out-of-plane acoustic phonons give larger contributions to thermal transport than in-plane acoustic modes despite broken reflection symmetry, important for determining the lifetimes of these modes. This work shows the important role that phonon dispersion features play in determining κ and demonstrates the potential for manipulating thermal transport in two dimensional materials via mass functionalization.

Acknowledgements

L. L. acknowledges support from the U. S. Department of Energy, Office of Science, Office of Basic Energy Sciences, Materials Sciences and Engineering Division and the National Energy Research Scientific Computing Center (NERSC), a DOE Office of Science User Facility

supported by the Office of Science of the U. S. Department of Energy under Contract No. DE-AC02-05CH11231.

References

- [1] K. S., Novoselov, A. K. Geim, S. V. Morozov, D. Jiang, Y. Zhang, S. V. Dubonos, I. V. Grigorieva, and A. A. Firsov, *Science* **306**, 666 (2004)
- [2] K. S. Novoselov, D. Jiang, F. Schedin, T. J. Booth, V. V. Khotkevich, S. V. Morozov, and A. K. Geim, *Proc. Natl Acad. Sci.* **102**, 10451 (2005).
- [3] A. K. Geim and K. S. Novoselov, *Nature Materials* **6**, 183 (2007).
- [4] B. Radisavljevic, A. Radenovic, J. Brivio, V. Giacometti, and A. Kis, *Nat. Nanotech.* **6**, 147 (2011).
- [5] H. Liu, A. T. Neal, Z. Zhu, Z. Luo, X. Xu, D. Tománek, and P. D. Ye, *ACS Nano* **8**, 4033 (2014).
- [6] Y. Zhang, J. W. Tan, H. L. Störmer, and P. Kim, *Nature* **438**, 201 (2005).
- [7] P. Vogt, P. De Padova, C. Quaresima, J. Avila, E. Frantzeskakis, M. C. Asensio, A. Resta, B. Ealet, and G. Le Lay, *Phys. Rev. Lett.* **108**, 155501 (2012).
- [8] A. J. Mannix, X.-F. Zhou, B. Kiraly, J. D. Wood, D. Alducin, B. D. Myers, X. Liu, B. L. Fisher, U. Santiago, J. R. Guest, M. J. Yacaman, A. Ponce, A. R. Oganov, M. C. Hersam, and N. P. Guisinger, *Science* **350**, 1513 (2015).
- [9] Q. H. Wang, K. Kalantar-Zadeh, A. Kis, J. N. Coleman, and M. S. Strano, *Nat. Nanotech.* **7**, 699 (2012).
- [10] T. Kuila, S. Bose, A. K. Mishra, P. Khanra, N. H. Kim, and J. H. Lee, *Prog. in Mat. Sci.* **57**, 1061 (2012).
- [11] M. F. Craciun, I. Khrapach, M. D. Barnes, and S. Russo, *J. Phys.: Cond. Mat.* **25**, 423201 (2013).

- [12] L. Yan, Y. B. Zheng, F. Zhao, S. Li, X. Gao, B. Xu, P. S. Weiss, and Y. Zhao, *Chem. Soc. Rev.* **41**, 97 (2012).
- [13] N. Lu, Z. Li, and J. Yang, *J. Phys. Chem. C* **113**, 16741 (2009).
- [14] M. A. Bissett, S. Konabe, S. Okada, M. Tsuji, and H. Ago, *ACS Nano* **7**, 10335 (2013).
- [15] A. A. Balandin, S. Ghosh, W. Bao, I. Calizo, D. Teweldebrhan, F. Miao, and C. N. Lau, *Nano Lett.* **8**, 902 (2008).
- [16] W. Cai, A. L. Moore, Y. Zhu, X. Li, S. Chen, L. Shi, and R. S. Ruoff, *Nano Lett.* **10**, 1645 (2010).
- [17] S. Chen, A. L. Moore, W. Cai, J. W. Suk, J. An, C. Mishra, C. Amos, C. W. Magnuson, J. Kang, L. Shi, and R. S. Ruoff, *ACS Nano* **5**, 321 (2011).
- [18] J.-U. Lee, D. Yoon, H. Kim, S. W. Lee, and H. Cheong, *Phys. Rev. B* **83**, 081419 (2011).
- [19] S. Chen, Q. Wu, C. Mishra, J. Kang, H. Zhang, K. Cho, W. Cai, A. A. Balandin, and R. S. Ruoff, *Nat. Mat.* **11**, 203 (2012).
- [20] J. H. Seol, I. Jo, A. L. Moore, L. Lindsay, Z. H. Aitken, M. T. Pettes, X. Li, Z. Yao, R. Huang, D. A. Broido, N. Mingo, R. S. Ruoff, and L. Shi, *Science* **328**, 213 (2010).
- [21] I. Jo, M. T. Pettes, L. Lindsay, E. Ou, A. Weathers, A. L. Moore, Z. Yao, and L. Shi, *AIP Advances* **5**, 053206 (2015).
- [22] L. Lindsay, D. A. Broido, and N. Mingo, *Phys. Rev. B* **82**, 115427 (2010).
- [23] L. Lindsay, D. A. Broido, and N. Mingo, *Phys. Rev. B* **83**, 235428 (2011).
- [24] D. Singh, J. Y. Murthy, and T. S. Fisher, *J. Appl. Phys.* **110**, 044317 (2011).
- [25] L. Lindsay, D. A. Broido, and N. Mingo, *Phys. Rev. B* **82**, 161402 (2010).
- [26] G. Fugallo, A. Cepellotti, L. Paulatto, M. Lazzeri, N. Marzari, and F. Mauri, *Nano Lett.* **14**, 6109 (2014).

- [27] A. Cepellotti, G. Fugallo, L. Paulatto, M. Lazzeri, F. Mauri, and N. Marzari, *Nat. Comm.* **6**, 6400 (2015).
- [28] P. Hohenberg and W. Kohn, *Phys. Rev.* **136**, B864 (1964).
- [29] W. Kohn and L. J. Sham, *Phys. Rev.* **140**, A1133 (1965).
- [30] <http://www.quantum-espresso.org>.
- [31] P. Gianozzi, S. Baroni, N. Bonini, M. Calandra, R. Car, C. Cavazzoni, D. Ceresoli, G. L. Chiarotti, M. Cococcioni, I. Dabo, A. D. Corso, S. Gironcoli, S. Fabris, G. Fratesi, R. Gebauer, U. Gerstmann, C. Gougoussis, A. Kokalj, M. Lazzeri, L. Matrin-Samo, *et. al.*, *J. Phys: Condens. Matter* **21**, 395502 (2009).
- [32] J. P. Perdew and A. Zunger, *Phys. Rev. B* **23**, 5048 (1981).
- [33] A. Dal Corso, S. Baroni, R. Resta, and S. de Gironcoli, *Phys. Rev. B* **47**, 3588 (1993).
- [34] J. C. Garcia, D. B. de Lima, L. V. C. Assali, and J. F. Justo, *J. of Phys. Chem. C* **115**, 13242 (2011).
- [35] P. Haas, F. Tran, and P. Blaha, *Phys. Rev. B* **79**, 085104 (2009).
- [36] L. Lindsay, D. A. Broido, and T. L. Reinecke, *Phys. Rev. B* **87**, 165201 (2013).
- [37] N. Mingo, D. A. Stewart, D. A. Broido, L. Lindsay, and W. Li, *Ab Initio Thermal Transport in Length-Scale Dependent Phonon Interactions* (Springer, Berlin, 2014).
- [38] J. Carrete, W. Li, L. Lindsay, D. A. Broido, L. J. Gallego, and N. Mingo, *Mat. Res. Lett.* **4**, 204 (2016).
- [39] W. H. Press, S. A. Teukolsky, W. T. Vetterling, and B. P. Flannery, *Numerical Recipes in Fortran* (Cambridge University Press, Cambridge, 1992).
- [40] G. Leibfried and W. Ludwig, *Solid State Phys.* **12**, 275 (1961).
- [41] K. Esfarjani and H. T. Stokes, *Phys. Rev. B* **77**, 144112 (2008).

- [42] M. Born and K. Huang, *Dynamical Theory of Crystal Lattices* (Clarendon Press, Oxford, 1998).
- [43] L. D. Landau and E. M. Lifshitz, *Theory of Elasticity*, Vol. 7, 3rd Ed. (Butterworth-Heinemann, Oxford, 1986).
- [44] K. H. Michel and B. Verberck, Phys. Rev. B **78**, 085424 (2008).
- [45] R. E. Peierls, *Quantum Theory of Solids* (Oxford University Press, London, 1955).
- [46] J. M. Ziman, *Electrons and Phonons* (Oxford University Press, London, 1960).
- [47] G. P. Srivastava, *The Physics of Phonons* (Taylor and Francis Group, New York, 1990).
- [48] Y. Kuang, L. Lindsay, and B. Huang, Nano Lett. **15**, 6121 (2015).
- [49] L. Lindsay, W. Li, J. Carrete, N. Mingo, D. A. Broido, and T. L. Reinecke, Phys. Rev. B **89**, 155426 (2014).
- [50] S. Mukhopadhyay, L. Lindsay, and D. J. Singh, Sci. Rep. **6**, 37076 (2016).
- [51] L. Lindsay, D. A. Broido, and T. L. Reinecke, Phys. Rev. Lett. **109**, 095901 (2012).
- [52] L. Lindsay, D. A. Broido, J. Carrete, N. Mingo, and T. L. Reinecke, Phys. Rev. B **91**, 121202 (2015).
- [53] A. Jain and A. J. H. McGaughey, J. App. Phys. **116**, 073503 (2014).
- [54] S. Lee, K. Esfarjani, T. F. Luo, J. W. Zhou, Z. T. Tian, and G. Chen, Nat. Comm. **5**, 3525 (2014).
- [55] S. Mukhopadhyay, L. Lindsay and D. S. Parker, Phys. Rev. B **93**, 224301 (2016).
- [56] L. Lindsay, Phys. Rev. B **94**, 174304 (2016).
- [57] Y. D. Kuang, L. Lindsay, S. Q. Shi, and G. P. Zheng, Nanoscale **8**, 3760 (2016).
- [58] S. I. Tamura, Phys. Rev. B **27**, 858 (1983).
- [59] L. Lindsay, D. A. Broido, and T. L. Reinecke, Phys. Rev. B **88**, 144306 (2013).

Table I. Calculated magnitude of phonon velocity, v , in the $\Gamma \rightarrow M$ direction for the LA (Γ) mode and the most dispersive optic branch at the M/2 point for select systems, as well as frequencies for the most dispersive optic branch at the Γ and M points. Also given are effective masses (defined in text) for the LA (M) mode and Γ and M modes of the most dispersive optic branch. Comparison of the calculated frequencies and velocities shown here is accurate to the given precision; however, numerical uncertainty in the calculation of the harmonic IFCs may reduce the overall precision.

	v (km/s) LA (Γ)	v (km/s) optic (M/2)	m_{eff} (amu) LA (M)	m_{eff} (amu) optic (Γ)	ω (THz) optic (Γ)	m_{eff} (amu) optic (M)	ω (THz) optic (M)
³ H	16.84	8.60	5.24	3.10	20.59	11.60	33.87
⁵ H	15.81	10.93	6.70	7.10	16.82	11.83	33.58
¹⁰ H	13.86	12.22	10.26	10.96	13.54	11.91	33.21
³⁰ H	9.98	12.75	29.76	17.19	10.81	13.04	33.00
⁶⁰ H	7.60	12.85	59.87	20.04	10.01	13.40	32.52
²⁰⁰ H	4.42	12.92	200.9	22.67	9.41	13.64	32.20

Table I

Figure Captions

Figure 1: Calculated room temperature κ for functionalized graphene versus functional group mass (black-dotted curve). The dashed red curve gives the κ contribution from acoustic modes, while the dashed blue curve gives that from optic modes. First principles calculated κ for graphane (purple square) and fluorographene (purple triangle) from Ref. 27 are also given. The inset shows the structure of these systems.

Figure2: Phonon dispersion of graphane ($C-^1H$; solid black curves), C-Deuterium ($C-^2H$; dashed red curves) and C-Tritium ($C-^3H$; dotted blue curves) in the $\Gamma \rightarrow M \rightarrow K \rightarrow \Gamma$ high symmetry directions.

Figure 3: Accumulated $\kappa(\omega)$ versus frequency for $C-^1H$ (blue curve), $C-^3H$ (black curve), $C-^5H$ (red curve), $C-^{10}H$ (green curve), $C-^{30}H$ (orange curve), $C-^{60}H$ (purple curve). Each curve is scaled by the corresponding calculated total κ for each system: 1718 W/m-K, 911 W/m-K, 637 W/m-K, 417 W/m-K, 284 W/m-K, 376 W/m-K, respectively. The maximum acoustic frequency for each system is marked by corresponding colored arrows. Accumulated $\kappa(\omega)$ is given by

$$\kappa(\omega) = \sum_{\bar{q}j} C_{\bar{q}j} v_{\bar{q}j\alpha}^2 \tau_{\bar{q}j\alpha} \theta(\omega - \omega_{\bar{q}j})$$
 where θ is the Heavyside step function, zero for $\omega - \omega_{\bar{q}j} < 0$ and

one for $\omega - \omega_{\bar{q}j} > 0$. Other terms are defined in the text.

Figure 4: Phonon dispersion of two highly dispersive optic branches and the LA branch in the $\Gamma \rightarrow M$ direction for $C\text{-}^3\text{H}$ (black curves), $C\text{-}^5\text{H}$ (red curves), $C\text{-}^{10}\text{H}$ (green curves), $C\text{-}^{30}\text{H}$ (orange curves) and $C\text{-}^{60}\text{H}$ (purples curves).

Figure 5: Calculated κ contributions for in-plane acoustic modes (green curve), out-of-plane acoustic modes (red curve) and optic modes (blue curve) versus functional group mass. Values are scaled by the total κ for each system. Also given is the calculated κ with phonon-isotope scattering from natural Carbon concentrations scaled by κ of the isotopically pure systems (black curve).

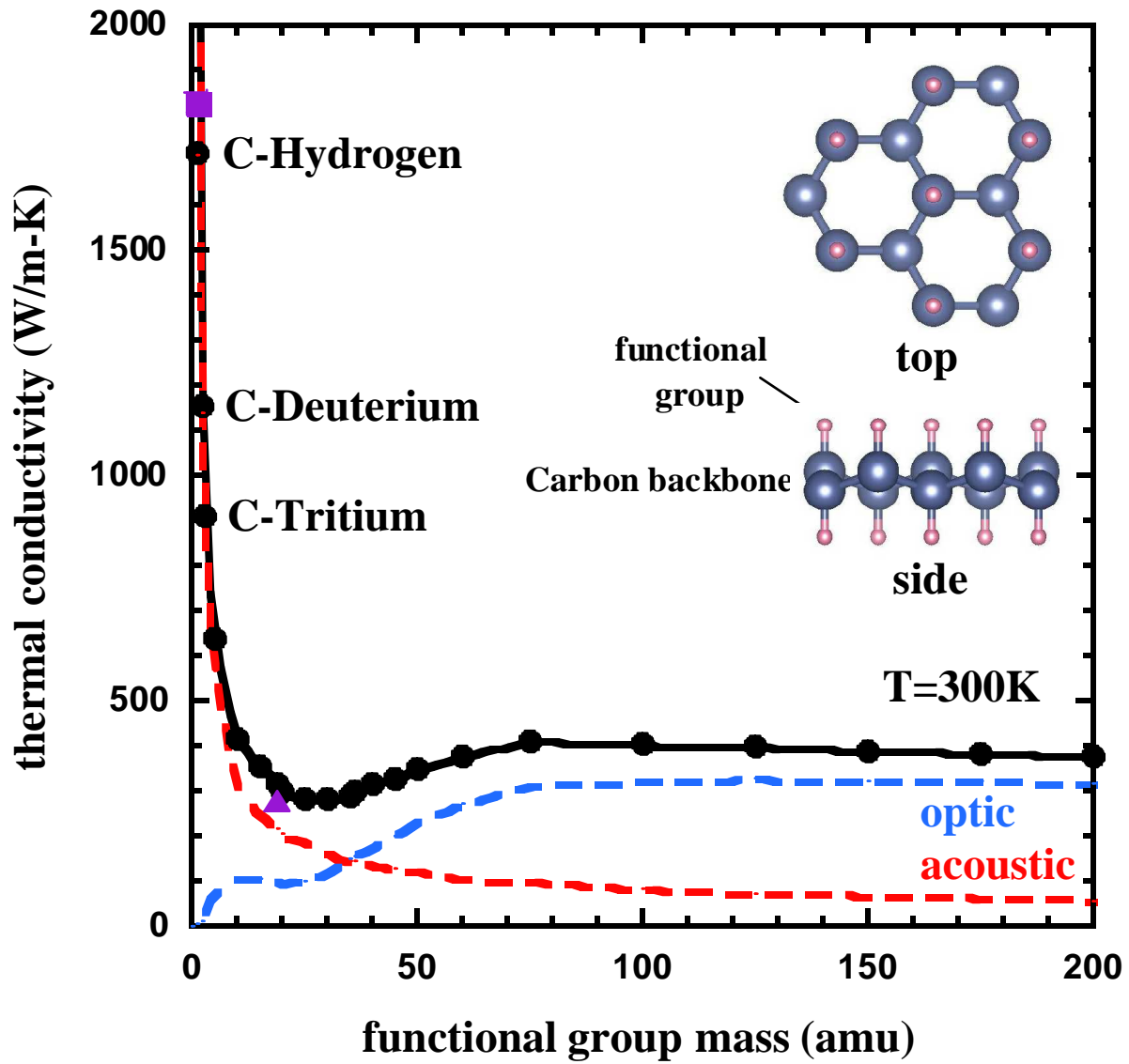


Figure 1

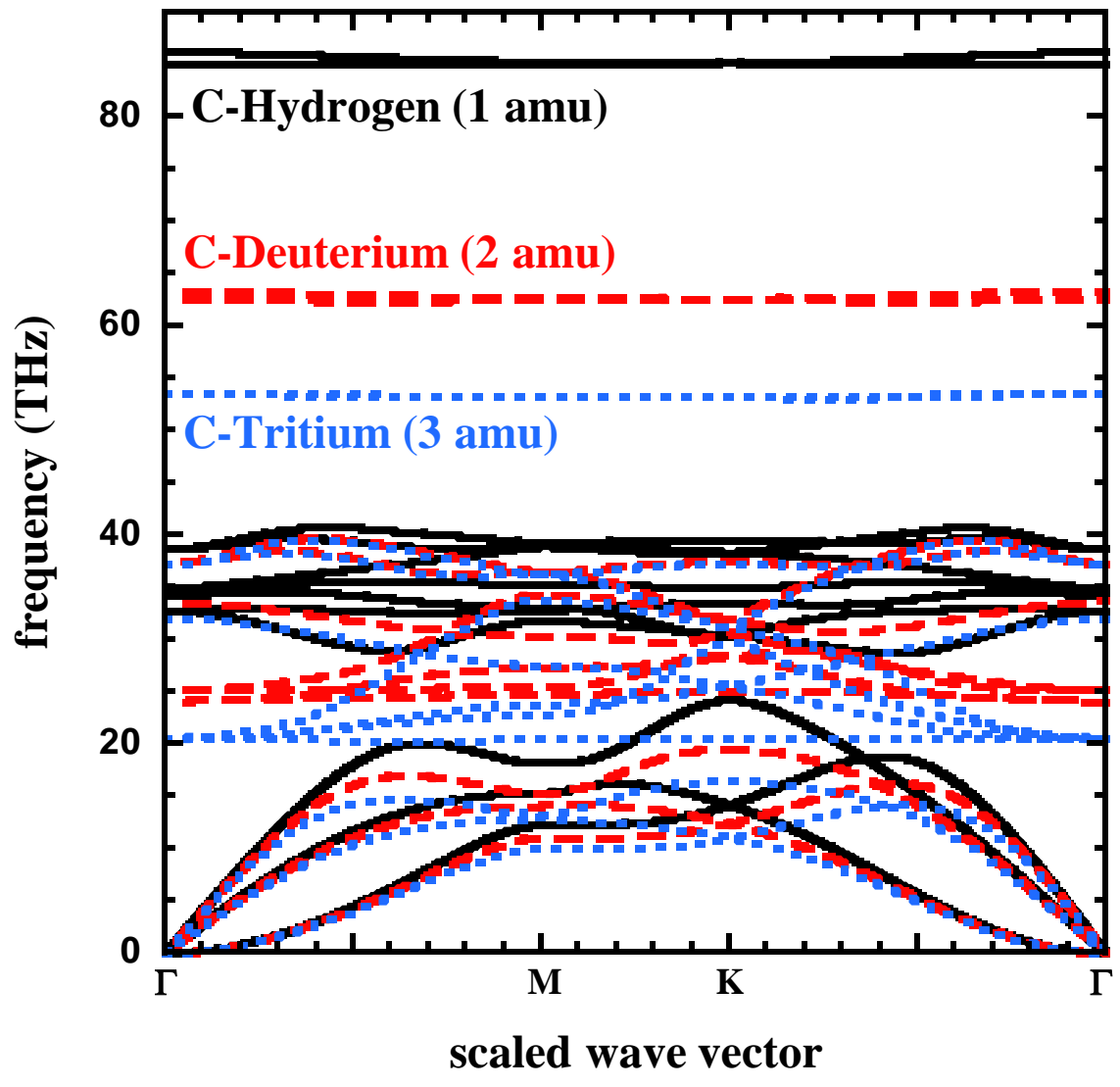


Figure 2

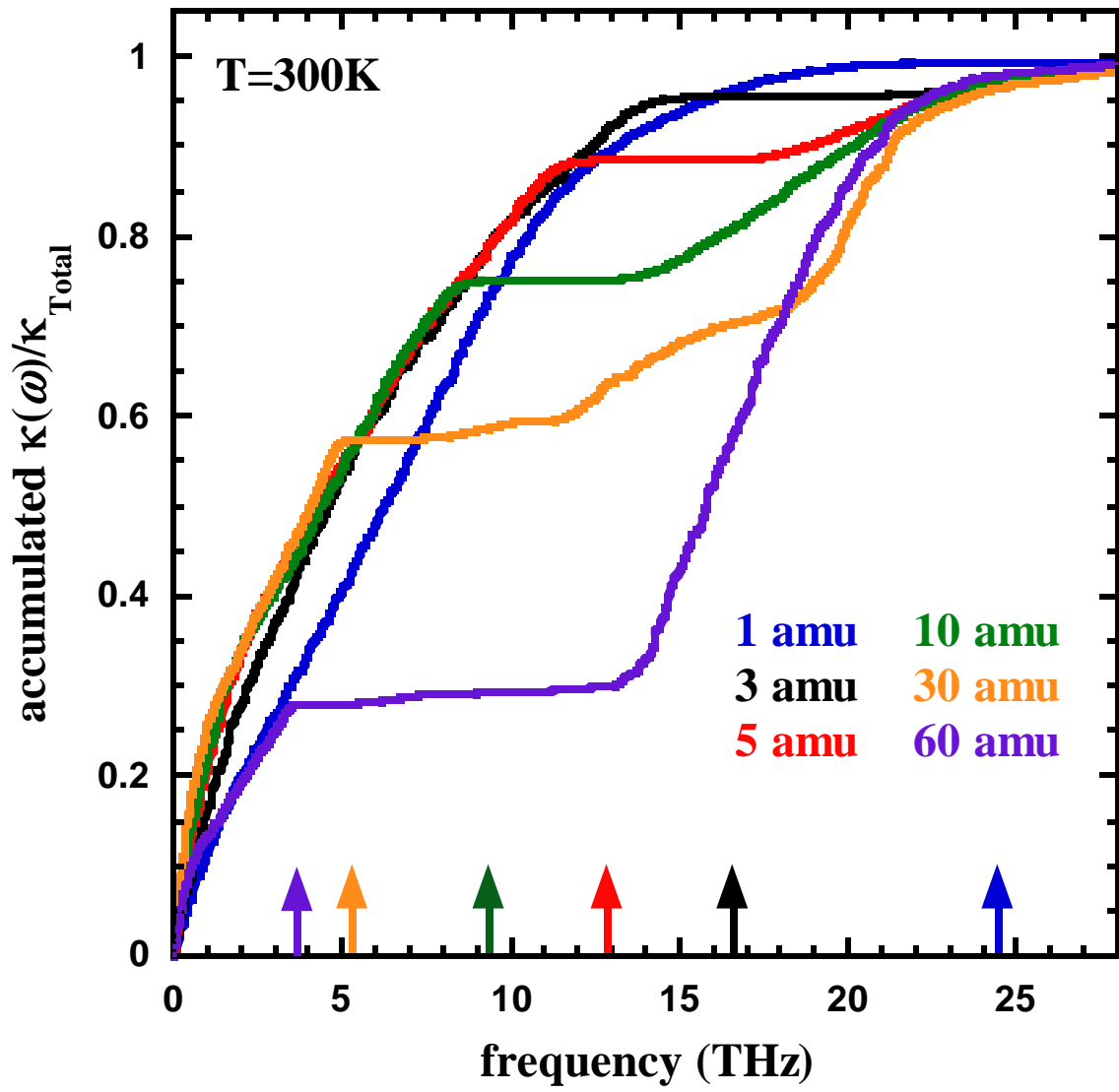


Figure 3

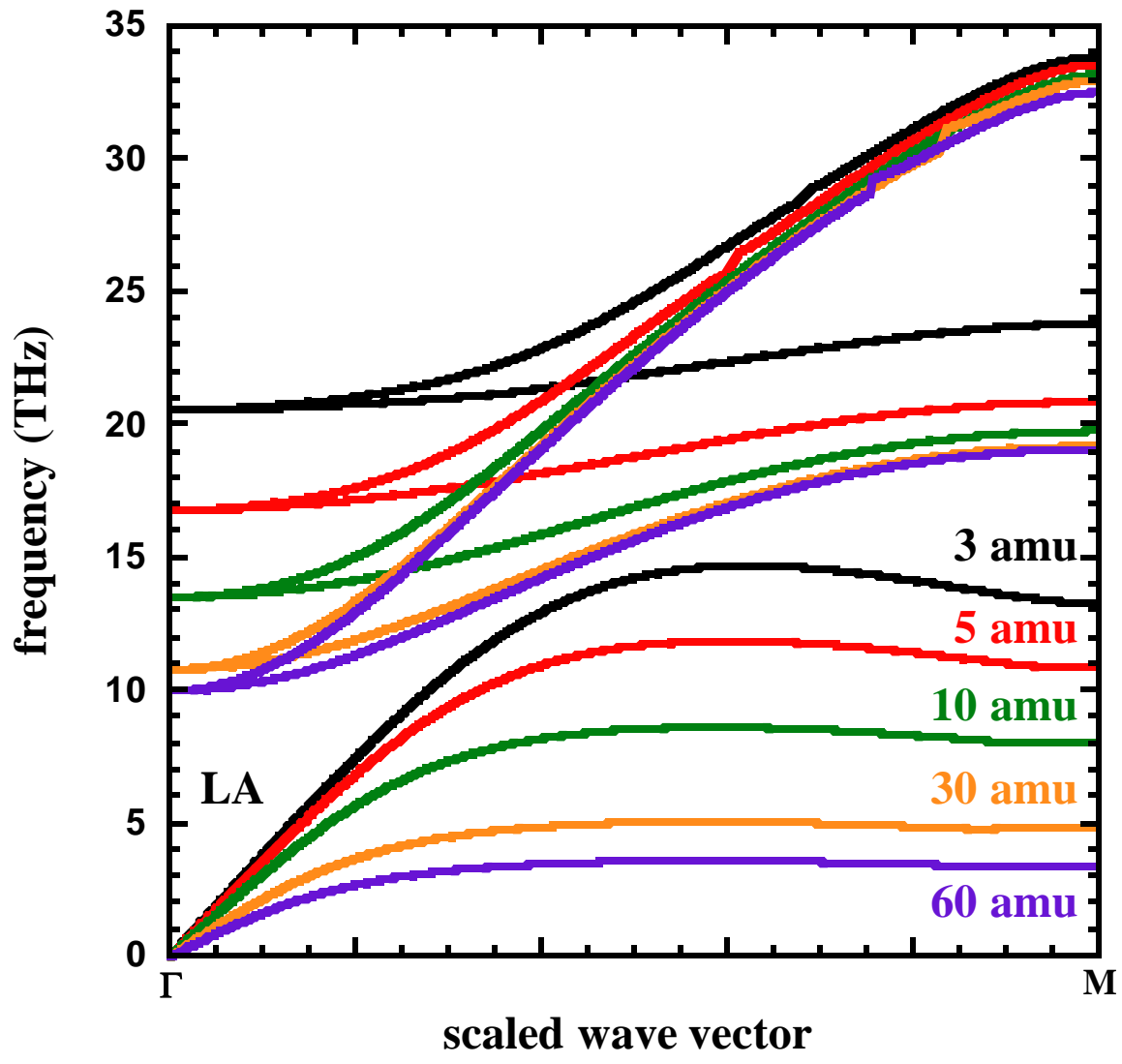


Figure 4

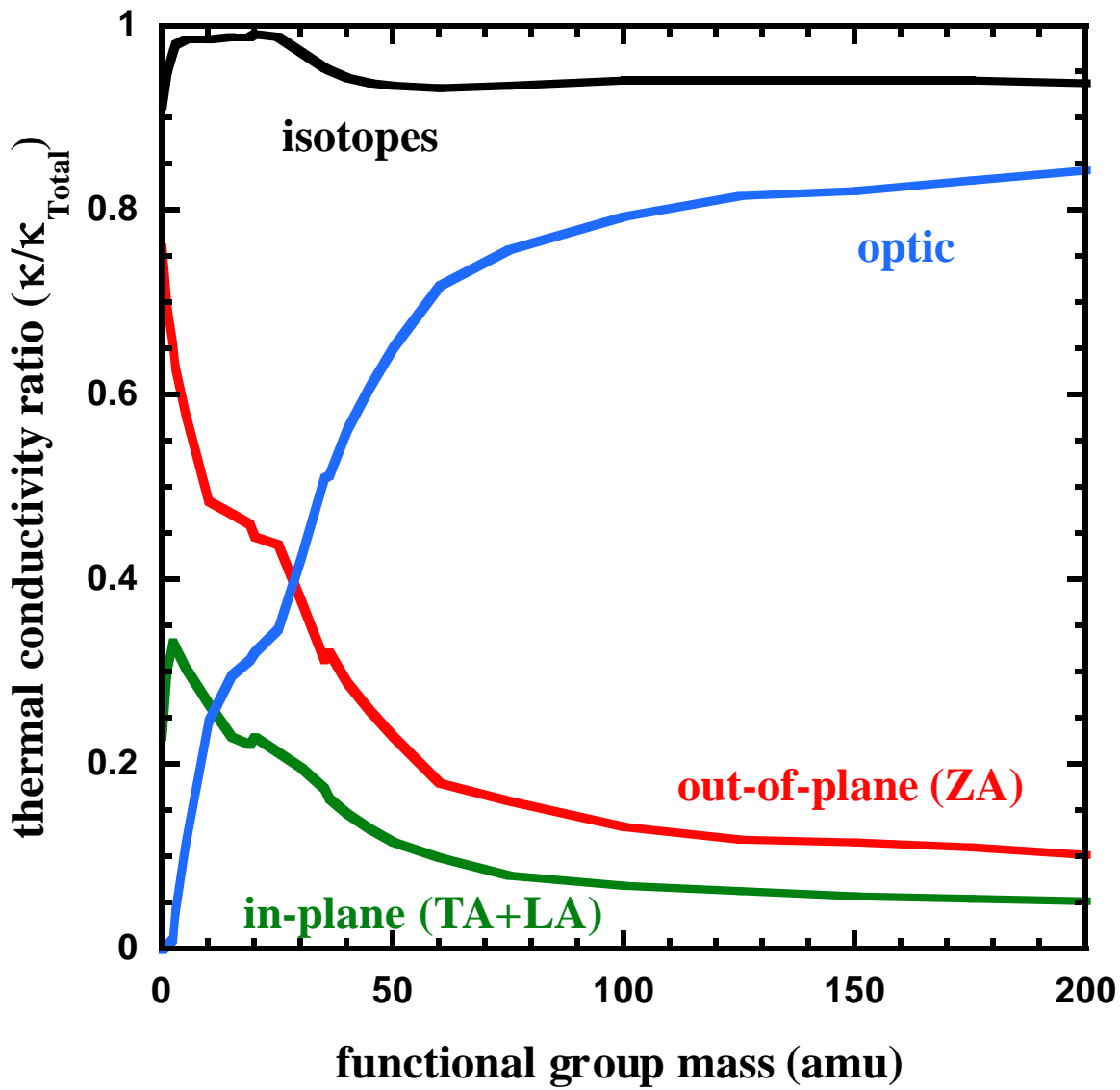


Figure 5